Robotics and Computer Integrated Manufacturing 57 (2019) 488–495

Contents lists available at ScienceDirect

Robotics and Computer Integrated Manufacturing

journal homepage: www.elsevier.com/locate/rcim

Full length Article

Prediction of surface roughness in extrusion-based additive manufacturing with machine learning

Zhixiong Li[a], Ziyang Zhang[a], Junchuan Shi[a], Dazhong Wu[b,*]

[a] Department of Mechanical and Aerospace Engineering, University of Central Florida, Orlando, FL, USA
[b] Department of Mechanical and Aerospace Engineering, Department of Industrial Engineering and Management Systems, University of Central Florida, Orlando, FL, USA

ARTICLE INFO

Keywords:
Fused filament fabrication
Monitoring
Predictive modeling
Surface roughness
Additive manufacturing

ABSTRACT

Additive manufacturing (AM), also known as 3D printing, has been increasingly adopted in the aerospace, automotive, energy, and healthcare industries over the past few years. While AM has many advantages over subtractive manufacturing processes, one of the primary limitations of AM is surface integrity. To improve the surface integrity of additively manufactured parts, a data-driven predictive modeling approach to predicting surface roughness in AM is introduced. Multiple sensors of different types, including thermocouples, infrared temperature sensors, and accelerometers, are used to collect temperature and vibration data. An ensemble learning algorithm is introduced to train the predictive model of surface roughness. Features in the time and frequency domains are extracted from sensor-based condition monitoring data. A subset of these features is selected to improve computational efficiency and prediction accuracy. The predictive model is validated using the condition monitoring data collected from a set of AM tests conducted on a fused filament fabrication (FFF) machine. Experimental results have shown that the proposed predictive modeling approach is capable of predicting the surface roughness of 3D printed components with high accuracy.

1. Introduction

Additive manufacturing (AM), also known as 3D printing, is an advanced manufacturing process that joins materials together in a layer-by-layer manner in order to create a three-dimensional object with a computer-aided design model [1]. AM techniques can be classified into seven categories: material extrusion, powder bed fusion, vat photopolymerization, material jetting, binder jetting, sheet lamination, and directed energy deposition. Fused filament fabrication (FFF), which is a material extrusion process, is one of the most widely used AM processes. FFF fabricates objects using a continuous filament of a thermoplastic material, which is heated in an extruder head, and then deposited onto a build plate [2].

While AM has been widely used for rapid prototyping, one of the limitations of AM is quality assurance and control [3–5]. For example, warping is one of the most common problems in AM due to material shrinkage which causes the corners of an object to lift and eventually detach from the build plate [2,6]. In addition, additively manufactured parts often have poor surface finish in comparison with subtractive manufacturing processes [7–9]. Surface roughness affects the tribological behavior of surfaces [10]. Because rough surfaces wear more quickly than smooth surfaces, it is very important to predict and control the surface roughness of additively manufactured parts [11–13]. Many factors such as layer thickness, print orientation and print speed affect surface roughness. This paper presents a novel online monitoring approach to predicting the surface roughness of 3D printed parts for FFF.

The remainder of the paper is organized as follows: Section 2 provides a review of the related work on process monitoring and surface roughness prediction. Section 3 introduces an ensemble learning-based approach to surface roughness prediction in AM. Section 4 presents an experimental setup. Section 5 presents experimental results and the performance of the predictive model. Section 6 provides conclusions and future work.

2. Related work

This section reviews current process monitoring techniques for FFF as well as the state-of-the-art in predictive modeling of surface roughness. Based on the literature review, a research gap in surface roughness prediction in AM is identified.

* Corresponding author
E-mail addresses: zhixiong.li@knights.ucf.edu (Z. Li), ziyang.zhang@Knights.ucf.edu (Z. Zhang), junchuan.shi@Knights.ucf.edu (J. Shi), Dazhong.Wu@ucf.edu (D. Wu).

https://doi.org/10.1016/j.rcim.2019.01.004
Received 3 October 2018; Received in revised form 7 January 2019; Accepted 7 January 2019

2.1. Process monitoring in FFF

According to several literature reviews on process monitoring of AM [14–17], pyrometers, thermocouples, displacement sensors and infrared (IR) imaging cameras have been widely used to monitor AM processes. Numerous research efforts have been devoted to detect defects by measuring temperatures, vibrations, optical emissions, and strains. Rao et al. [18] introduced an online monitoring method for failure detection in the FFF process. A set of AM tests was conducted on a desktop 3D printer instrumented with multiple sensors such as thermal couples, accelerometers, and an infrared temperature sensor. Experimental results have shown that this method was capable of detecting failure modes with very high accuracy. Zhao and Rosen [19] developed a data-driven method that can monitor an exposure controlled projection lithography process. This method was demonstrated on real-time condition monitoring data. Experimental results have shown that the data mining method can predict the height profile of cured parts. Kousiatza and Karalekas [20] developed an online monitoring system that predicts strain and temperature profiles using health condition data generated by thermocouples and optical sensors. Residual strains were measured using Fiber Bragg grating sensors. Specimens were fabricated on a FFF printer. Experimental results have shown that the proposed approach is capable of predicting residual strains and temperatures with high accuracy.

2.2. Surface roughness prediction

Galantucci et al. [21] studied the effects of various machining parameters on the surface roughness of 3D printed parts. A set of tests was conducted to study the effects of layer thickness and raster width on surface roughness. Boschetto et al. [22] developed a predictive modeling approach to estimating the surface roughness of parts built by FFF. The predictive modeling approach was demonstrated on a set of experiments. Boschetto and Bottini [23] developed a model that can estimate the surface roughness of the parts built by FFF and barrel finishing operations. The analytical model was validated using a set of experimental datasets. Reeves and Cobb [24] developed an analytical model of the surface roughness of the parts built by the stereolithography process. The effects of layer thickness, surface angle, layer profile angle, up-facing layer composition, and down-facing layer composition on surface roughness were studied. Ahn et al. [6] developed a method to predict the surface roughness of 3D printed parts based on the geometric data in an STL file. Multiple specimens were fabricated on an SLA 3500 machine. The surface roughness of these specimens was measured with a profilometer. Experimental results have shown that the prediction accuracy of the model is less than one micrometer.

In summary, while previous studies have attempted to develop various techniques in order to estimate surface roughness in AM processes, little research has been reported on predicting surface roughness in AM with heterogeneous sensors and data-driven methods. To fill this research gap, a novel data-driven predictive modeling approach based on machine learning is introduced to predict the surface roughness of additively manufactured components in FFF.

3. Predictive modeling of surface roughness

Fig. 1 illustrates the data-driven predictive modeling method which involves offline model training and online prediction. Training data were collected from in-situ sensors that measure the build plate temperature and vibrations, the extruder temperature and vibration, and the temperature of the deposited material. A set of features in the time and frequency domains was extracted from the raw signals. A subset of the features was selected based on their importance determined by random forests. The subset of features was fed into the ensemble learning algorithm to build a predictive model of surface roughness. The predictive model will then be used for online prediction. As shown in Table 1, the ensemble learning algorithm combines six different base learners, including RF, AdaBoost, classification and regression trees (CART), support vector regression (SVR), ridge regression (RR), and random vector functional link (RVFL) network.

The base learning algorithms are combined using the following weighted function:

$$\hat{\mathbf{P}} = \sum_{j=1}^{J} w_j \mathbf{P}_j, \tag{1}$$

where $\hat{\mathbf{P}} = [\hat{P}^1, \hat{P}^2, ..., \hat{P}^N]$ denotes the output of the algorithm, N is the number of samples. $\mathbf{P}_j = [P_j^1, P_j^2, \ldots, P_j^N]$ denotes the output of the jth base learner, J is the number of base learners. w_j denotes the weight of the jth base learner. The optimal weights assigned to the base learners are determined using the sequential quadratic optimization (SQP) method [25]. The cost function is described as follows:

$$\begin{cases} \min\limits_{\mathbf{w}} \delta = e(\hat{\mathbf{P}} - \bar{\mathbf{P}}) \\ Subject\ to\ \sum_{j=1}^{J} w_j = 1 \end{cases}, \tag{2}$$

where $\bar{\mathbf{P}}$ denotes the actual surface roughness (ground truth), $e(\cdot)$ is a predefined error that measures the accuracy of the ensemble learning algorithm.

3.1. Random forests

RF is an ensemble learning algorithm that constructs a multitude of uncorrelated regression trees [26–28]. To develop a regression tree, a splitting and a stopping criterion are required. To determine the best split at each node, the following objective function needs to be solved:

$$\min_{j,\,s}\left[\min_{c1}\sum_{x_i \epsilon R_1(j,s)}(y_i - c1)^2 + \min_{c2}\sum_{x_i \epsilon R_2(j,s)}(y_i - c2)^2\right], \tag{3}$$

where y_i is the response variable of i^{th} sample x_i. $j = 1, 2, ..., p$, (p denotes the number of splitting variables). s denotes a cutting point. $R_1(j, s) = \{X|X_j \le s\}$ and $R_2(j, s) = \{X|X_j \ge s\}$ denote two resulting regions after the best split is determined. X_j denotes the j^{th} splitting variable. $c1 = ave(y_i|x_i \epsilon R_1(j, s))$ denotes the average of the y_i's that fall into the region $R_1(j, s)$. $c2 = ave(y_i|x_i \epsilon R_2(j, s))$ denotes the average of the y_i's that fall into the region $R_2(j, s)$. The process of splitting a parent node into two child nodes is repeated until a stopping criterion is satisfied. In this paper, when the number of samples in a node falls below a threshold, which is 10, the splitting process will be stopped. The random forest consists of 500 regression trees.

3.2. AdaBoost

AdaBoost (i.e., Adaptive Boosting) is an ensemble learning algorithm in which weak learners are combined into a weighted sum [29]. AdaBoost is an algorithm for constructing a strong learner as a linear combination of weak learners:

$$H(x) = \text{sign}\left(\sum_{k=1}^{K} \alpha_k h_k(x)\right), \tag{4}$$

where $h_k(x)$ denotes the kth weak learner, K is the number of weak learners, α_k denotes the coefficient of the kth weak learner, and $H(x)$ denotes a strong learner. To determine the optimal coefficients α_k, the initial weight for a learner is updated after an iteration based on the error associated with the learner. First, initialize weights $D_i(i) = 1/m$, m is the number of samples. Second, train K weak learners and assign a greater coefficient to the one with better performance. Third, assign a greater weight for the training sample with a greater error. Forth, repeat the second and third steps to optimize the coefficients of the K

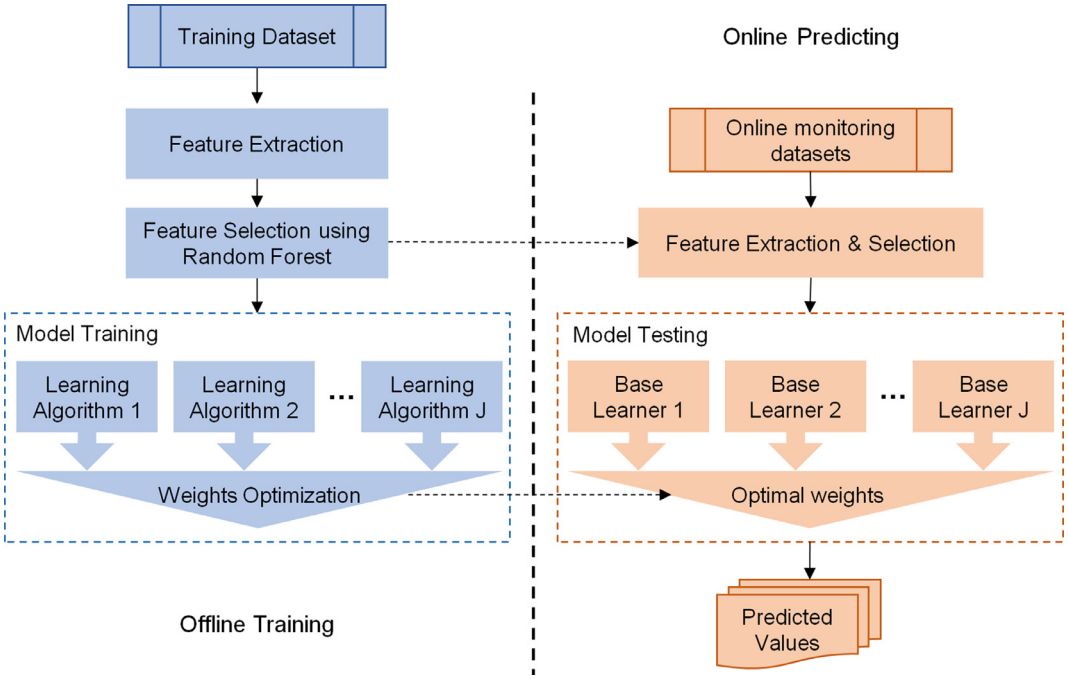

Fig. 1. A data-driven predictive modeling approach to predicting surface roughness.

Table 1
Base learner selection.

Category	Selected algorithm
Decision tree-based	Classification and regression trees (CART)
Neural network-based	Random vector functional link (RVFL) network
Regularization-based	Ridge regression (RR)
	Support vector regression (SVR)
Ensemble-based	Random forests (RF)
	AdaBoost

weak learners. Last, combine the weak learners to create a strong learner. In this study, the decision tree model was used as the weak learners and $K = 300$. RMSE was used to assess the error.

3.3. Classification and regression tree

CART is an algorithm that builds decision trees for making predictions [30]. CART starts at a root node and then splits the node into children nodes based on the least squares error criterion. This recursive splitting process will continue until a stopping criterion is satisfied. A typical stopping criterion is to stop splitting a node when the number of samples in the node is less than five (5).

3.4. Support vector regression

SVR is a machine learning algorithm that solves the following convex optimization problem [31,32]:

Minimize

$$\frac{1}{2}\|\omega\|^2 + C\sum_{i=1}^{\ell}(\xi_i + \xi_i^*), \tag{5}$$

Subject to

$$\begin{cases} y_i - \langle \omega, x_i \rangle - b \le \varepsilon + \xi_i \\ \langle \omega, x_i \rangle + b - y_i \le \varepsilon + \xi_i^* \\ \xi_i, \xi_i^* \ge 0 \end{cases}$$

where $C > 0$ determines the tradeoff between the flatness of the function $f(x) = \langle \omega, x \rangle + b$ and the amount up to which deviations larger than ε are tolerated. Kernel functions such as polynomial, Gaussian radial basis function (RBF), and sigmoid have been extensively used to transform data to new data in a higher dimension such that the data are separable [32,33]. In this paper, the Gaussian RBF kernel was used to transform the original dataset into a new dataset in a higher dimensional space. The slack variables ξ_i and ξ_i^* denote the deviation from predicted values with an error of ε. The solution to the optimization problem described above is given by

$$\omega = \sum_{i=1}^{\ell}(\alpha_i - \alpha_i^*)\Phi(x), \tag{6}$$

$$f(x) = \sum_{i=1}^{\ell}(\alpha_i - \alpha_i^*)k(x_i, x_j) + b, \tag{7}$$

$b = y_i - \langle \omega, x_i \rangle - \varepsilon$ for $\alpha_i \in [0, C]$ or $b = y_i - \langle \omega, x_i \rangle + \varepsilon$ for $\alpha_i^* \in [0, C]$

3.5. Ridge regression

RR is an algorithm that conducts L_2 regularization (i.e., L_2-penalty) by imposing a penalty that is determined by the sum of square of regression coefficients [33]. RR minimizes the following objective function:

$$\hat{\beta}^{ridge} = \underset{\beta}{\operatorname{argmin}}\left\{\sum_{i=1}^{N}\left(y_i - \beta_0 - \sum_{j=1}^{Q} x_{ij}\beta_j\right)^2 + \lambda\sum_{j=1}^{Q}\beta_j^2\right\}, \tag{8}$$

where β_j is a regression coefficient, $\hat{\beta}^{ridge}$ is the optimal regression coefficients, $\lambda \ge 0$ is a tuning parameter that controls the coefficients, N is the number of samples, x_{ij} is the covariate with a dimension of N by Q, y_i is the response variable. The optimization problem above can be solved by

$$\hat{\beta}^{ridge} = (\boldsymbol{X}^T\boldsymbol{X} + \lambda \mathrm{I})^{-1}\boldsymbol{X}^T y. \tag{9}$$

where $\mathbf{I}$ is a $Q \times Q$ identity matrix. If $\boldsymbol{X}$ is replaced with its kernel vector $\boldsymbol{\Phi}$, Eq. (9) can be rewritten as

$$\hat{\beta}^{ridge} = (\boldsymbol{\Phi}^T\boldsymbol{\Phi} + \lambda \mathrm{I})^{-1}\boldsymbol{\Phi}^T y. \tag{10}$$

where the kernel vector $\mathbf{\Phi}$ is a matrix of a kernel function $k(x_i, x_j) := \langle \Phi(x_i), \Phi(x_j) \rangle$. In this study, the kernel function $k(x_i, x_j) = exp(-\frac{\arccos(x_i - x_j)^2}{2\sigma^2})$ where $\sigma^2 = 0.5$ was used.

3.6. Random vector functional link network

Random vector functional link (RVFL) network [34] is a new type of single layer feed forward neural network (SLFN). RVFL has a similar structure to classical SLFN. However, in addition to the neuron connections between hidden and output layers, RVFL has direct neuron connections between input and output layers. The weights between input and hidden layers are randomly generated. The output of RVFL is represented as

$$o_i = \boldsymbol{F}_i \omega \tag{11}$$

where o_i ($i = 1, 2, \ldots, N$, N is the number of samples) is the prediction of the ith sample, $\boldsymbol{F}_i$ is the matrix version of the assembly of the original inputs and the outputs of the hidden layer for the ith sample, and $\boldsymbol{\omega}$ is the weights of the output layer. The learning algorithm, such as the regularized least square, is used to estimate $\boldsymbol{\omega}$ by minimizing the prediction error E.

$$\arg\min_{\omega} E = \sum_{i}^{N} (y_i - o_i)^2 + \epsilon \|\omega\|^2, \tag{12}$$

where y_i is the response variable of ith sample and ϵ is a small positive constant. In this study, ten neurons were used in the hidden layer. The regularized least square algorithm was used to train the network.

4. Experimental setup

Fig. 2 shows an experimental setup. The specimens were fabricated on a commercial desktop 3D printer (MakerBot Replicator Plus). The build material was Polylactic Acid (PLA). To collect condition monitoring data, the 3D printer was instrumented with five sensors. Two thermocouples were used to measure the temperature of the build plate and extruder, respectively. Two accelerometers were used to measure the vibration of the build plate and extruder. An IR non-contact temperature sensor was used to measure the temperature of the deposited material. Table 2 lists the details about the sensors and measurements.

After printing a specimen, the surface roughness of the specimen was measured with a profilometer. A profilometer measures small surface variations in vertical stylus displacement as a function of position. Roughness average (Ra) was used to quantify surface roughness. Fig. 3(a) shows the CAD model of an engine intake flange. Fig. 3(b) shows where surface roughness was measured.

To validate the predictive model, we conducted a full factorial experiment with three factors as shown in Table 3. Each factor has three levels. Each AM test was replicated three times. Eighty-one (81) tests were conducted. Table 4 shows the experimental data. Sensor-based condition monitoring data were collected from ten (10) signal channels during each test. Fig. 4 shows the extruder temperature and build plate vibration signals.

Table 2
Sensor specification and measurement.

Sensor specification	Measurement
Thermocouple 1 (5TC-GG-K-20-36, Omega)	Build plate temperature
Thermocouple 2 (5TC-GG-K-20-36, Omega)	Extruder temperature
Accelerometer 1 (ADXL335, Analog Devices)	Build plate vibration
Accelerometer 2 (ADXL335, Analog Devices)	Extruder vibration
IR Temperature Sensor (MLX90614, Melexis Technologies NV)	Melt pool temperature

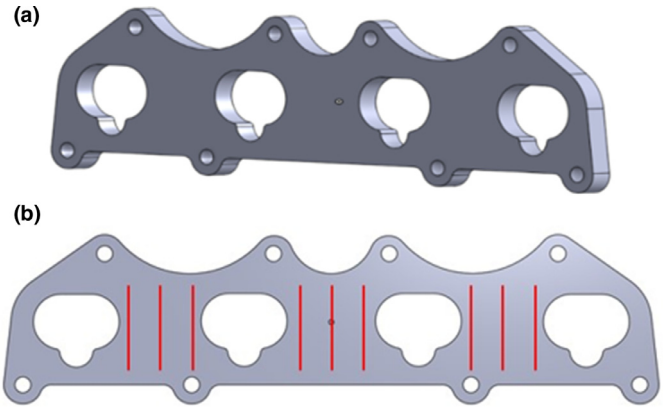

Fig. 3. (a) CAD model of the engine intake flange; (b) measurement of surface roughness.

Table 3
Experimental design.

Factor	Level 1	Level 2	Level 3
Layer thickness (mm)	0.20	0.25	0.30
Extruder temperature (°C)	210	220	230
Print speed/extrusion rate	0.85	1.00	1.15

5. Results and discussions

We extracted eight (8) statistical features (i.e., maximum, median, mean, minimum, standard deviation, central moment, skewness and kurtosis) in the time domain from each signal channel. In addition, we extracted four (4) features in the frequency domain, including maximum, median, mean and minimum of the spectral-amplitude, from the vibration sensors using a fast Fourier transform (FFT) algorithm. A total number of 104 features was extracted from each test. In order to improve computational efficiency as well as to avoid overfitting, a subset of the features was selected based on feature importance calculated using the RF algorithm. Fig. 5 shows the prediction accuracy with varying number of selected features. As shown in Fig. 5, predicting surface roughness with more features does not necessarily increase prediction accuracy. This is because some of the features are either

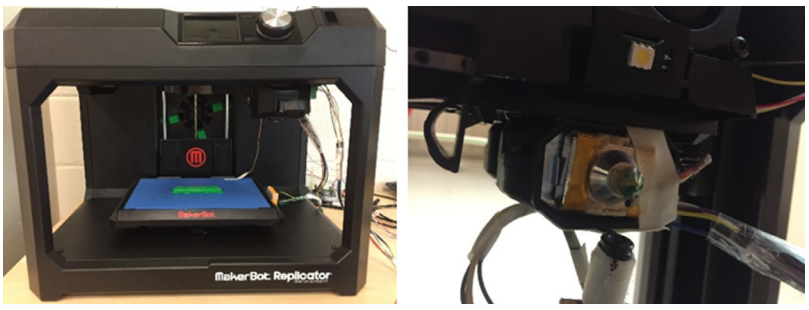

Fig. 2. Experimental setup.

Table 4
Experimental data.

ID	Feed rate to Flow rate	Layer thickness (mm)	Extruder temperature (°C)	Roughness (um)	Roughness (um)	Roughness (um)
1	1	0.3	210	5.972	6.056	5.898
2	1	0.3	230	6.183	6.152	6.062
3	1	0.3	220	6.296	6.319	6.234
4	1	0.25	210	4.995	5.032	5.080
5	1	0.25	230	5.613	5.715	5.709
6	1	0.25	220	5.664	5.436	5.142
7	1	0.2	210	4.146	4.569	4.820
8	1	0.2	230	5.565	4.758	4.987
9	1	0.2	220	4.925	4.724	5.314
10	0.85	0.3	210	5.989	5.791	6.172
11	0.85	0.3	230	6.124	6.240	6.155
12	0.85	0.3	220	5.828	6.299	6.006
13	0.85	0.25	210	5.184	5.258	5.238
14	0.85	0.25	230	5.359	5.453	5.582
15	0.85	0.25	220	5.498	5.421	5.427
16	0.85	0.2	210	4.414	4.476	4.589
17	0.85	0.2	230	5.619	5.342	5.907
18	0.85	0.2	220	4.750	4.888	5.038
19	1.15	0.3	210	5.918	5.749	5.975
20	1.15	0.3	230	6.217	6.327	6.251
21	1.15	0.3	220	5.729	6.155	6.223
22	1.15	0.25	210	5.142	5.086	5.489
23	1.15	0.25	230	5.359	5.749	5.379
24	1.15	0.25	220	5.267	5.311	5.390
25	1.15	0.2	210	4.626	4.623	4.445
26	1.15	0.2	230	5.354	5.306	5.357
27	1.15	0.2	220	5.151	4.953	4.936

redundant or irrelevant. Removing these irrelevant features will not reduce but instead improve prediction accuracy. The experimental results have shown that the predictive model built by the ensemble learning algorithm with forty (40) features outperforms those trained with 20, 60, 80, and 104 features. Therefore, forty (40) out of 104 features were selected to train the predictive model. Table 5 lists top five (5) most important features based on their importance. These features include (a) the maximum frequency amplitude of the build plate vibration, (b) the maximum extruder vibration in the Z direction, (c) the standard deviation of the build plate temperature, (d) the minimum melt pool temperature, and (e) the skewness of the extruder vibration in the Y direction. More details about feature importance assessment can be referred to Grömping [35].

The performance of the predictive models was measured using root-mean-square-error (RMSE) and relative error (RE). The predictive models were trained on a portion of the total data, and then tested on the remaining data. For example, one of the predictive models was trained on 50% of the raw data, and then tested on the rest 50% of the raw data.

Fig. 6 shows the RMSE and RE of the predictive model trained on 50% of the total samples (training sample size: 40). The performance ranking of the base learners is RR, SVR, CART, RF, RVFL, and AdaBoost

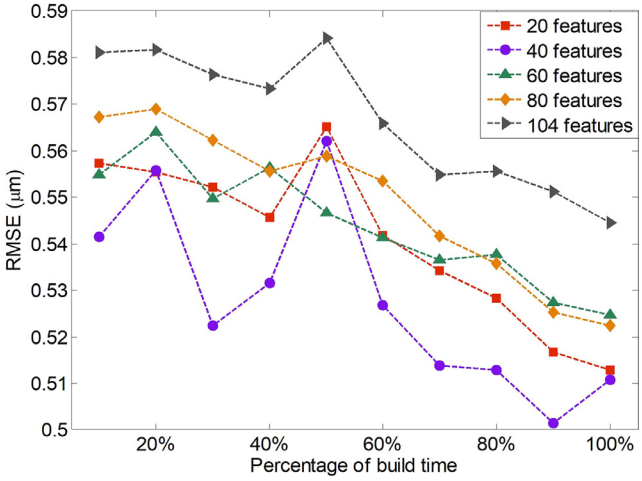

Fig. 5. Impact of feature selection on the accuracy of the predictive models (Training data: 50% of the experimental data).

Table 5
Top 5 most important features.

Rank	Feature	Importance
1	Max frequency amplitude of build plate vibration (Y)	0.162
2	Max extruder vibration (Z)	0.159
3	Standard deviation of build plate temperature	0.144
4	Mini melt pool temperature	0.096
5	Skewness of extruder vibration (Y)	0.091

based on both RMSE and RE. The performance of CART is comparable to the performance of RF. Similarly, the performance of RR is close to the performance of SVR. As expected, the ensemble learning algorithm outperforms the individual base learners. Moreover, the predictive models were tested on the data collected during a time interval ranging from 10% to 100% of the build time. As shown in Fig. 6, except for AdaBoost, the individual base learners and the ensemble can predict surface roughness in real-time with high accuracy (RMSE: 0.7 μm; RE: 0.1) when the elapsed time is only a small percentage of the total build time. For example, the RMSEs of RF, AdaBoost, CART, SVR, RR, and RVFL tested on the data collected by the time 20% of the part was built are 0.652, 0.859, 0.644, 0.563, 0.569, and 0.692, respectively, whereas the RMSE of the ensemble method is 0.566 μm. Increasing the amount of test data does not improve the performance of the base learners and the ensemble significantly. Table 6 lists the RMSEs and REs of the predictive models trained by the based learners and the ensemble learning algorithm. Fig. 7 shows the actual and predicted surface roughness for 41 test datasets. The test data were collected when 50% of the total build time elapsed.

Similarly, Fig. 8 shows the RMSE and RE of the predictive model trained on 70% of the total samples (training sample size: 56). The performance ranking of the base learners is RF, RR, SVR, CART, AdaBoost, and RVFL based on both RMSE and RE. The performance of RF is

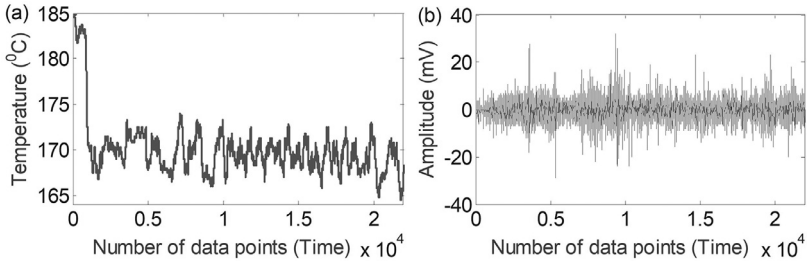

Fig. 4. Sensor-based measurements: (a) extruder temperature and (b) build plate vibrations (*Y* direction).

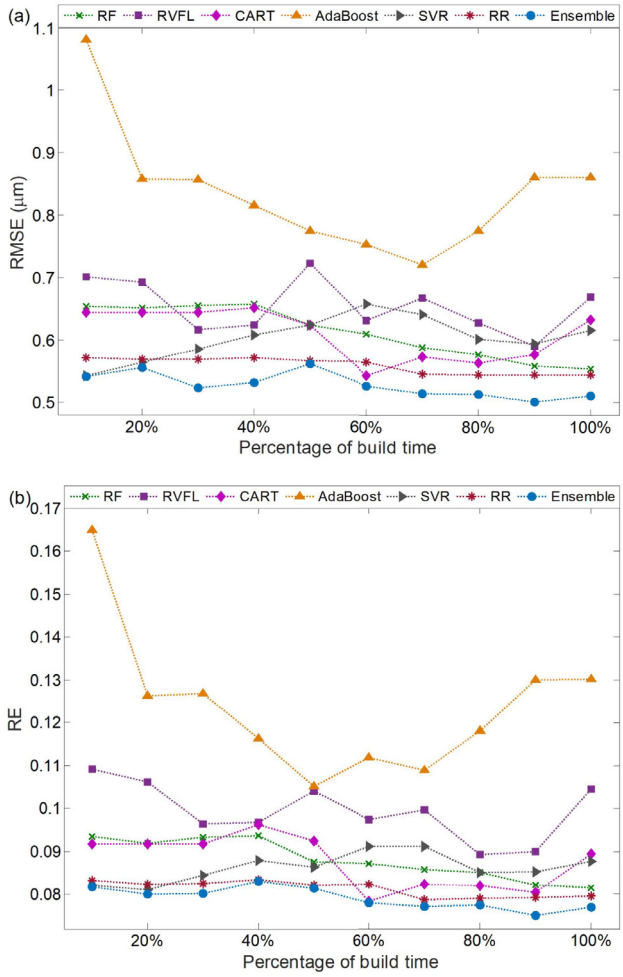

Fig. 6. Accuracy of the predictive models on test data (training data: 50% of the experimental data): (a) RMSE and (b) RE.

comparable to the performance of RR and SVR. The ensemble learning algorithm still outperforms the individual base learners. Fig. 9 shows the actual and predicted surface roughness for 25 test datasets. The test data were collected by the time when 50% of the total build time elapsed.

Fig. 10 shows the RMSE and RE of the predictive model trained on 90% of the total samples (training sample size: 72). The performance ranking of the base learners is SVR, RR, RF, CART, RVFL, and AdaBoost based on both RMSE and RE. The performance of SVR is comparable to the performance of RR and RF. Again, the ensemble learning algorithm outperforms the individual base learners. Fig. 11 shows the actual and predicted surface roughness for nine test datasets. The test data were collected by the time when 50% of the total build time elapsed.

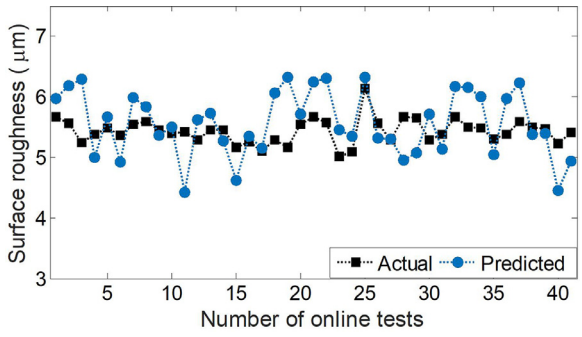

Fig. 7. Actual vs predicted surface roughness using 50% of the experimental data collected from 41 samples.

Table 7 shows the RMSE and RE of the models trained on 50%–90% of the total data. These models were tested on the data collected by the time when 20%–100% of the total build time elapsed. Table 8 lists the optimal weights assigned to the base leaners. AdaBoost was not used in any of the ensembles because its weight was zero. The weights assigned to RF are greater because RF outperformed other base learners.

Our findings suggest that the surface roughness of the 3D printed specimens primarily depends on the frequency amplitude of the build plate vibrations, the extruder vibrations, the temperature of the build plate, and the melt pool temperature. In addition, the experimental results have shown that the predictive models trained by the ensemble learning algorithm is capable of predicting surface roughness of 3D printed parts in real-time given condition monitoring data and surface roughness measurements. The existing methods predict surface roughness using process parameters such as layer thickness and build direction, whereas the predictive modeling method introduced in this paper predicts surface roughness using sensor-based condition monitoring data. The ensemble learning algorithm boosts six weak learners to a stronger one, which makes better predictions.

6. Conclusions and future work

This paper has presented an ensemble learning-based approach to surface roughness prediction in FFF processes. Multiple sensors were used to collect real-time condition monitoring data. A set of features in the time and frequency domains were extracted from the raw sensor-based signals. To improve computational efficiency as well as to avoid overfitting, a subset (40) of the features was selected using RF based on feature importance. The predictive models were trained using the ensemble learning algorithm. The ensemble learning algorithm combined six different machine learning algorithms, including RF, AdaBoost, CART, SVR, RR, and RVFL network. The experimental results have shown that the predictive models are capable of predicting the surface roughness of the 3D printed specimens. The performance of the ensemble outperforms the individual base learners based on RMSE and RE. In the future, the proposed approach will be used to predict the

Table 6
Online prediction performance (Training data: 50% of the experimental data).

Error	Percentage of build time	RF	AdaBoost	CART	SVR	RR	RVFL	Ensemble
RMSE	20%	0.652	0.859	0.644	0.563	0.569	0.692	0.556
	40%	0.658	0.816	0.652	0.608	0.571	0.624	0.532
	60%	0.61	0.753	0.543	0.658	0.566	0.632	0.527
	80%	0.577	0.776	0.563	0.601	0.545	0.627	0.513
	100%	0.554	0.86	0.633	0.616	0.545	0.669	0.511
RE	20%	0.092	0.126	0.092	0.081	0.082	0.106	0.08
	40%	0.094	0.116	0.096	0.088	0.083	0.097	0.083
	60%	0.087	0.112	0.078	0.091	0.082	0.097	0.078
	80%	0.085	0.118	0.082	0.085	0.079	0.089	0.077
	100%	0.081	0.13	0.09	0.088	0.08	0.105	0.077

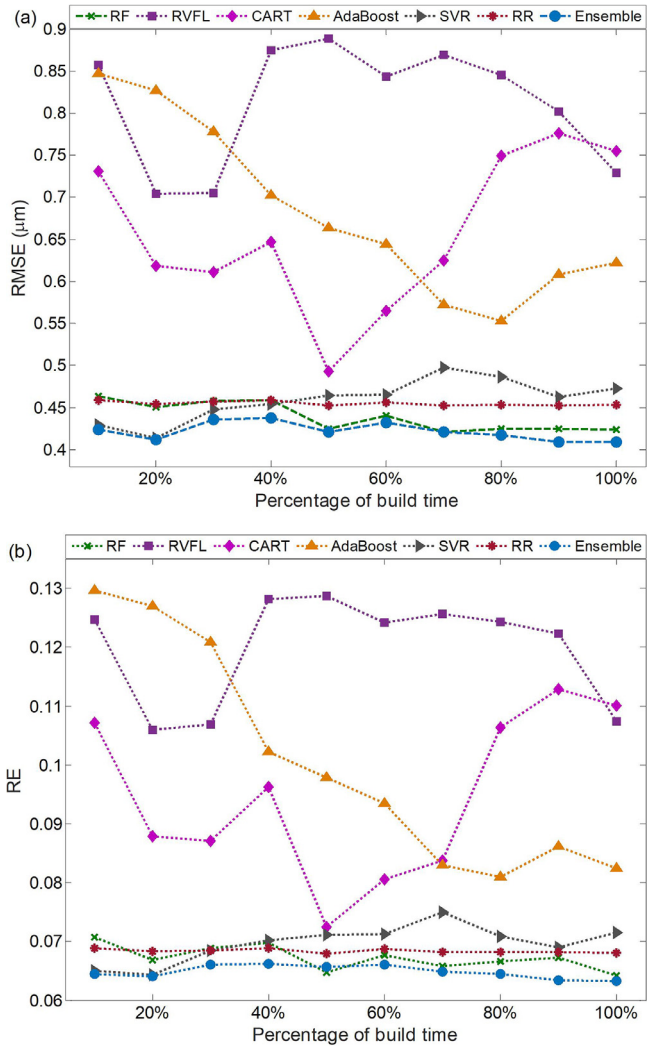

Fig. 8. Accuracy of the predictive models on test data (training data: 70% of the experimental data): (a) RMSE and (b) RE.

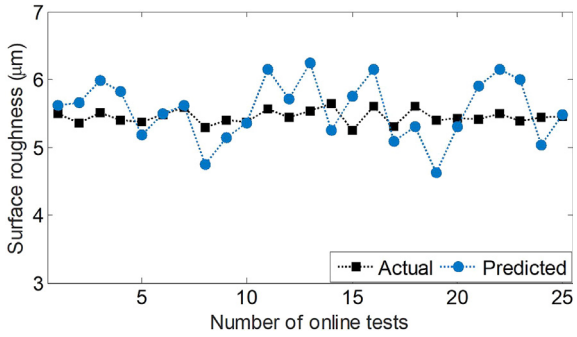

Fig. 9. Actual vs predicted surface roughness using 50% of the experimental data collected from 25 samples.

surface roughness of additively manufactured components in selective laser sintering and electron beam melting.

Acknowledgments

The research reported in this paper is partially supported by the University of Central Florida (UCF) and the Digital Manufacturing and Design Innovation Institute (DMDII) (Grant No. DMDII-15-14-01). Any opinions, findings, and conclusions or recommendations expressed in this paper are those of the authors and do not necessarily reflect the views of the UCF and the DMDII. We thank Stephen Rey and Brooke Mansfield for proofreading the paper.

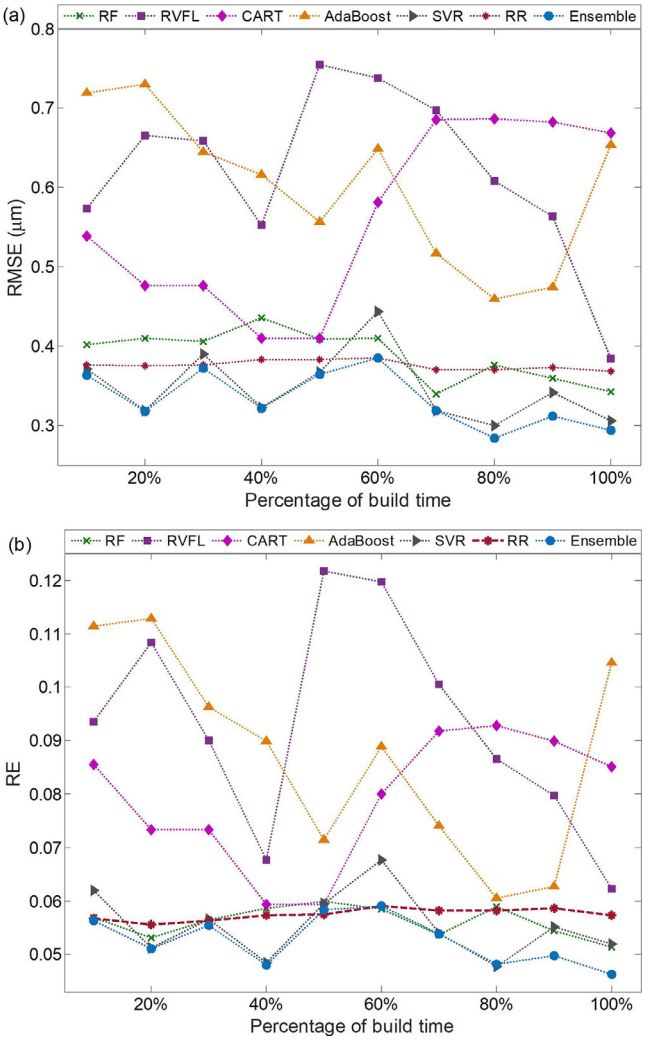

Fig. 10. Accuracy of the predictive models on test data (training data: 90% of the experimental data): (a) RMSE and (b) RE.

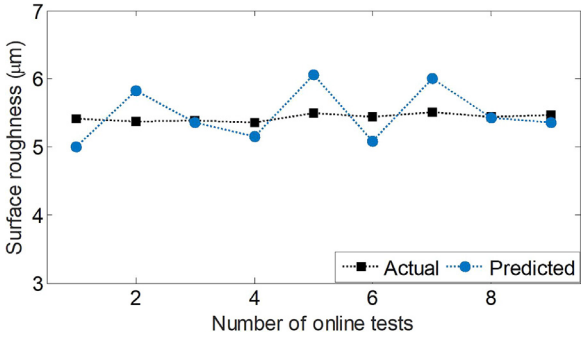

Fig. 11. Actual vs predicted surface roughness using 50% of the experimental data collected from 9 samples.

Supplementary materials

Supplementary material associated with this article can be found, in the online version, at doi:10.1016/j.rcim.2019.01.004.

Table 7
Effect of training data size on prediction accuracy.

Training data size	RMSE				
	20%	40%	60%	80%	100%
50%	0.556	0.532	0.527	0.513	0.511
60%	0.496	0.496	0.484	0.465	0.476
70%	0.414	0.448	0.440	0.424	0.438
80%	0.365	0.355	0.401	0.405	0.406
90%	0.318	0.321	0.385	0.284	0.294
Training data size	RE				
50%	0.080	0.083	0.078	0.077	0.077
60%	0.074	0.074	0.070	0.059	0.062
70%	0.064	0.066	0.066	0.065	0.063
80%	0.048	0.047	0.060	0.061	0.061
90%	0.051	0.048	0.059	0.048	0.046

Table 8
Weights assigned to base learners.

Training data size	Optimal weights					
	RF	RVFL	CART	AdaBoost	SVR	RR
50%	0.056	0.002	0.107	0.000	0.003	0.832
60%	0.786	0.000	0.130	0.000	0.084	0.000
70%	0.582	0.000	0.000	0.000	0.169	0.249
80%	0.537	0.003	0.000	0.000	0.145	0.315
90%	0.819	0.000	0.000	0.000	0.181	0.000

References

[1] D.L. Bourell, M.C. Leu, D.W. Rosen, Roadmap for Additive Manufacturing: Identifying the Future of Freeform Processing, The University of Texas at Austin, Austin, TX, 2009, pp. 11–15.
[2] T. Srivatsan, T. Sudarshan, Additive Manufacturing: Innovations, Advances, and Applications, CRC Press, 2015.
[3] M. Asadi-Eydivand, M. Solati-Hashjin, A. Farzad, N.A.A. Osman, Effect of technical parameters on porous structure and strength of 3D printed calcium sulfate prototypes, Rob. Comput. Integr. Manuf. 37 (2016) 57–67.
[4] X. Zhang, B. Zhou, Y. Zeng, P. Gu, Model layout optimization for solid ground curing rapid prototyping processes, Rob. Comput. Integr. Manuf. 18 (1) (2002) 41–51.
[5] L.M. Galantucci, F. Lavecchia, G. Percoco, Experimental study aiming to enhance the surface finish of fused deposition modeled parts, CIRP Ann. 58 (1) (2009) 189–192.
[6] D. Ahn, H. Kim, S. Lee, Surface roughness prediction using measured data and interpolation in layered manufacturing, J. Mater. Process. Technol. 209 (2) (2009) 664–671.
[7] H.-S. Byun, K.H. Lee, Determination of the optimal build direction for different rapid prototyping processes using multi-criterion decision making, Rob. Comput. Integr. Manuf. 22 (1) (2006) 69–80.
[8] B.N. Turner, S.A. Gold, "A review of melt extrusion additive manufacturing processes: II. Materials, dimensional accuracy, and surface roughness, Rapid Prototyping J. 21 (3) (2015) 250–261.
[9] G. Strano, L. Hao, R.M. Everson, K.E. Evans, Surface roughness analysis, modelling and prediction in selective laser melting, J. Mater. Process. Technol. 213 (4) (2013) 589–597.
[10] F. Calignano, D. Manfredi, E. Ambrosio, L. Iuliano, P. Fino, Influence of process parameters on surface roughness of aluminum parts produced by DMLS, Int. J. Adv. Manuf. Technol. 67 (9-12) (2013) 2743–2751.
[11] P. Benardos, G.C. Vosniakos, Prediction of surface roughness in CNC face milling using neural networks and Taguchi's design of experiments, Rob. Comput. Integr. Manuf. 18 (5-6) (2002) 343–354.
[12] N. Abburi, U. Dixit, A knowledge-based system for the prediction of surface roughness in turning process, Rob. Comput. Integr. Manuf. 22 (4) (2006) 363–372.
[13] D. Wu, Y. Wei, J. Terpenny, Predictive modeling of surface roughness in fused deposition modeling using data fusion, Int. J. Prod. Res. (2019), https://doi.org/10.1080/00207543.2018.1505058.
[14] G. Tapia, A. Elwany, A review on process monitoring and control in metal-based additive manufacturing, J. Manuf. Sci. Eng. 136 (6) (2014) 060801.
[15] S.K. Everton, M. Hirsch, P. Stravroulakis, R.K. Leach, A.T. Clare, Review of in-situ process monitoring and in-situ metrology for metal additive manufacturing, Mater. Des. 95 (2016) 431–445.
[16] W.E. Frazier, Metal additive manufacturing: a review, J. Mater. Eng. Perform. 23 (6) (2014) 1917–1928.
[17] E.W. Reutzel, A.R. Nassar, A survey of sensing and control systems for machine and process monitoring of directed-energy, metal-based additive manufacturing, Rapid Prototyping J. 21 (2) (2015) 159–167.
[18] P.K. Rao, J.P. Liu, D. Roberson, Z.J. Kong, C. Williams, Online real-time quality monitoring in additive manufacturing processes using heterogeneous sensors, J. Manuf. Sci. Eng. 137 (6) (2015) 061007.
[19] X. Zhao, D.W. Rosen, A data mining approach in real-time measurement for polymer additive manufacturing process with exposure controlled projection lithography, J. Manuf. Syst. 43 (2017) 271–286.
[20] C. Kousiatza, D. Karalekas, In-situ monitoring of strain and temperature distributions during fused deposition modeling process, Mater. Des. 97 (2016) 400–406.
[21] L.M. Galantucci, F. Lavecchia, G. Percoco, Experimental study aiming to enhance the surface finish of fused deposition modeled parts, CIRP Ann. Manuf. Technol. 58 (1) (2009) 189–192.
[22] A. Boschetto, V. Giordano, F. Veniali, 3D roughness profile model in fused deposition modelling, Rapid Prototyping J. 19 (4) (2013) 240–252.
[23] A. Boschetto, L. Bottini, Roughness prediction in coupled operations of fused deposition modeling and barrel finishing, J. Mater. Process. Technol. 219 (2015) 181–192.
[24] P.E. Reeves, R.C. Cobb, Reducing the surface deviation of stereolithography using in-process techniques, Rapid Prototyping J. 3 (1) (1997) 20–31.
[25] J.-F. Bonnans, J.C. Gilbert, C. Lemaréchal, C.A. Sagastizábal, Numerical Optimization: Theoretical and Practical Aspects, Springer Science & Business Media, 2013.
[26] L. Breiman, Random forests, Mach. Learn. 45 (1) (2001) 5–32.
[27] A. Liaw, M. Wiener, Classification and regression by randomForest, R News 2 (3) (2002) 18–22.
[28] D. Wu, C. Jennings, J. Terpenny, R.X. Gao, S. Kumara, A comparative study on machine learning algorithms for smart manufacturing: tool wear prediction using random forests, J. Manuf. Sci. Eng. 139 (7) (2017) 071018.
[29] Y. Freund, R.E. Schapire, A decision-theoretic generalization of on-line learning and an application to boosting, J. Comput. Syst. Sci. 55 (1) (1997) 119–139.
[30] J. Friedman, T. Hastie, R. Tibshirani, The Elements of Statistical Learning, Springer Series in Statistics, New York, 2001.
[31] C. Cortes, V. Vapnik, Support-vector networks, Mach. Learn. 20 (3) (1995) 273–297.
[32] A. Smola, V. Vapnik, "Support vector regression machines, Adv. Neural Inf. Process. Syst. 9 (1997) 155–161.
[33] A.E. Hoerl, R.W. Kennard, Ridge regression: biased estimation for nonorthogonal problems, Technometrics 12 (1) (1970) 55–67.
[34] L. Zhang, P.N. Suganthan, A comprehensive evaluation of random vector functional link networks, Inf. Sci. 367 (2016) 1094–1105.
[35] U. Grömping, Variable importance assessment in regression: linear regression versus random forest, Am. Stat. 63 (4) (2009) 308–319.